

## PHOTOMETRIC CHARACTERIZATION OF SELECTED LUNAR SITES BY SMART-1 AMIE DATA.

V. Kaydash<sup>1</sup>, M. Kreslavsky<sup>1</sup>, Yu. Shkuratov<sup>1</sup>, S. Gerasimenko<sup>1</sup>, P. Pinet<sup>2</sup>, S. Chevrel<sup>2</sup>, J.-L. Josset<sup>3</sup>, S. Beauvivre<sup>3</sup>, M. Almeida<sup>4</sup>, B. Foing<sup>4</sup>, <sup>1</sup>Astronomical Institute of Kharkov Natl. University, Sumskaya 35, Kharkov, 61022 Ukraine. kvg@vk.kh.ua, <sup>2</sup>UMR 5562/CNRS/ Toulouse III University, Midi-Pyrenees Observatory, 14 Av. E. Belin, 31400 Toulouse, France. <sup>3</sup>Space Exploration Institute (Case postale, CH-2002 Neuchâtel, Switzerland) <sup>4</sup>ESA/ESTEC (Keplerlaan 1, 2201 Noordwijk, The Netherlands)

**Introduction:** Optical properties of the lunar surface are formed in the upper mm-thick layer of regolith and thus bear information about the regolith structure. We use images obtained in 2006 by Advanced Moon Micro-Imager Experiment (AMIE) camera onboard SMART-1 spacecraft to access photometric properties of selected lunar areas in the context of geological and structural properties of the regolith. We map the steepness of phase function for several areas and find local peculiarities of the function. These anomalies are discussed in terms of regolith microstructure.

**Model of the lunar phase function:** Photometric function of the Moon describes the dependence of lunar surface brightness on incidence  $i$ , emergence  $e$  and phase  $\alpha$  angles. Following [1] we use an approximation of photometric function proposed by Akimov [2], which was successfully applied to NASA Clementine data [1]. This approximation expresses the photometric function through the phase angle  $\alpha$ , photometric latitude  $\beta$  and longitude  $\lambda$  and can be factorized on two multipliers: the first is the phase function dependent solely on  $\alpha$ ; the second is the so-called disk function dependent on  $\beta$  and  $\lambda$ , i.e. on the orientation of the scattering surface to the Sun and observer for given  $\alpha$ :

$$F(\alpha, \beta, \lambda) = \exp(-\eta\alpha) \cos(\alpha/2) \times \frac{[\cos(\lambda - \alpha/2)]^{\nu\alpha+1} - [\sin(\alpha/2)]^{\nu\alpha+1}}{(\lambda - [\sin(\alpha/2)]^{\nu\alpha+1}) \cos \lambda} (\cos \beta)^{\nu\alpha} \quad (1)$$

This formula contains only two adjustable parameters, the parameter of disk function  $\nu$  and the steepness of phase function  $\eta$ . Thus we apply this description to SMART-1 lunar data in order to map the photometric function parameters and analyze lunar photometrical properties using the maps obtained.

**AMIE multiangular photometric data:** During the SMART-1 mission, a number of color (750, 915 and 960 nm) and wideband (no-filter) lunar images were obtained with the AMIE micro-imager. Spatial resolution of the images (1024x1024 pixels in size, dynamic range of 1023 DN) varies from tens to hundreds of meters. The AMIE data set gives access, with a selection of targeted observations using spot pointing, to the phase function determination and search for photometric anomalies [3].

**Data processing:** The preliminary pipeline calibration [4] allows accounting for Master Flat fields and Master Dark frames depending on exposure time and

temperature of the detector. With this procedure, we convert raw counts to the values proportional to the bidirectional reflectance under given illumination/ observation conditions, which is sufficient to make phase-ratios and normalized phase dependence of brightness. It has been shown that the preliminary calibration gives reasonable image ratios even in color filters [5]. However the SNR is highest for images taken in no-filter (512x512 pixels) area, therefore in this study we deal with the “blank” filter images. Images of the same scene obtained at different geometries are specially coregistered with subpixel accuracy to compensate the differences in camera pointing and the field-of-view curvature; for this we have applied an autocorrelation procedure for subpixel transformations of image data. Then we calculate photometric angles ( $\alpha$ ,  $\beta$ ,  $\lambda$ ) for each pixel in the same scene images. The local surface tilts (surface topography) disturb the values of  $\beta$  and  $\lambda$ , therefore, our method is presently valid for flat areas only (mare, crater floors etc.).

**Mapping the photometric function parameters:** Knowing the reflectance and photometric angles, we apply least squares fit procedure to find the parameter of phase function  $\eta$  in Eq. (1). We run this algorithm several times for different fixed values of the disk function parameter  $\nu$  and found that disk function vary slightly for a wide range of  $\nu$ , therefore, parameter  $\nu$  does not affect spatial pattern of  $\eta$  maps affecting only the absolute values of  $\eta$ . Finally, we adopt  $\nu=0.3$  in accordance with previous studies [6].

**Gruithuisen domes.** The first area (centered at 39.5 W, 35.8 N) we studied covers Gruithuisen domes and surrounding mare in the western part of Mare Imbrium. Five successive images were obtained in the SMART-1 orbit 2236. Photometric angles for these data are  $i = 45^\circ$ ,  $e = 4-30^\circ$ ,  $\alpha = 30-70^\circ$ ; the resolution varies from 110 to 160 m/pix. Fig. 1a presents a part of an image of this area, a map of the parameter  $\eta$  is shown in Fig. 1b. Major apparent variations of the phase function steepness parameter are associated with surface tilts and look like illuminated topography in Fig. 1b. The map also reveals detectable true photometric variations associated with small craters in a mare unit where previous spectral analysis indicates the presence of MS2-like regolith [7]. Arrows 1 in Fig.1 mark two craters with high  $\eta$  values (“positive”

photometric anomaly) and arrows 2 point to two craters with diffuse extended halos of low  $\eta$  (“negative” anomaly); these halos have no albedo expression. Similar crater-related negative anomalies were observed in other sites with Clementine data [6].

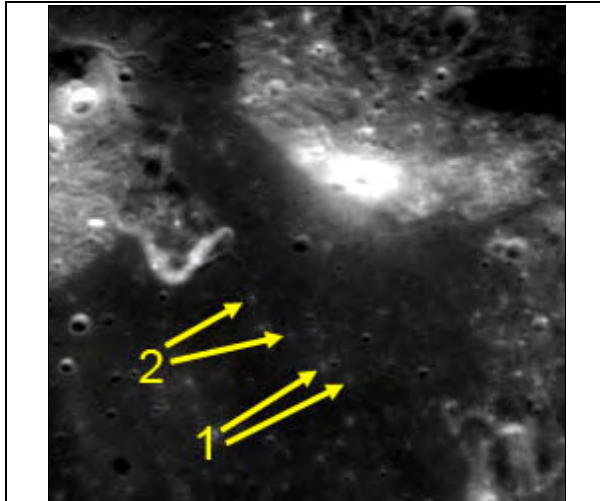


Fig. 1a. Reflectance image of Gruithuisen Hills area. Arrows show areas with photometric anomalies.

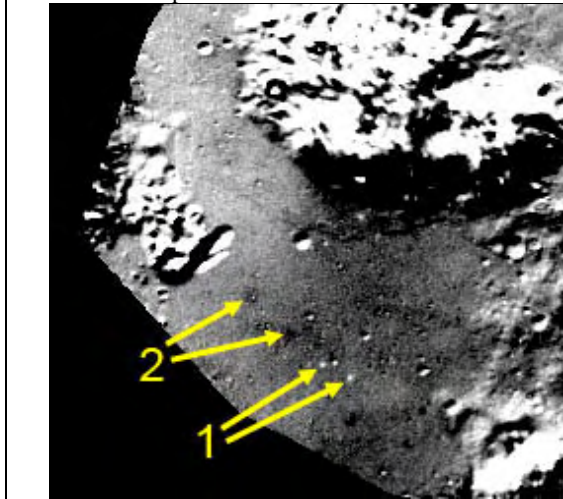


Fig. 1b. Map of the parameter  $\eta$  (phase function steepness). Brighter tones correspond to higher values of  $\eta$  (i.e. steeper phase function).

The negative anomaly for distal ejecta areas may be explained by disturbing the “fairy-castle” microstructure of the regolith by the impact event. The local modification can produce a less porous layer with suppressed shadow-hiding effect [6]. We interpret the positive anomaly for craters 1 as an increase of mesoscale roughness in the proximal ejecta zone, making the phase function steeper. This roughness can be due to the presence of an anomalously large number of boulders and blocks. Such photometric anomalies were not observed in areas studied in [6]. Large-scale subtle variations of  $\eta$  over the mare surface (Fig.1b) may be

explained by the presence of more fine-grained pyroclastic material in the vicinity of volcanic domes.

**Crater Lavoisier.** Another spot-pointing AMIE campaign was carried out for the orbit 2251; 33 shots of the cracked-floor crater Lavoisier (80.8 W, 38.2 N; Fig. 2a) were made. Photometric angles are  $e = 0-45^\circ$ ,  $\alpha = 26-80^\circ$ ; while  $i = 45^\circ$ , the resolution varies from 110 to 200 m/pix. The  $\eta$  parameter map in Fig. 2b highlights the absence of dark areas at the periphery of the crater floor (cf. Fig. 2a).

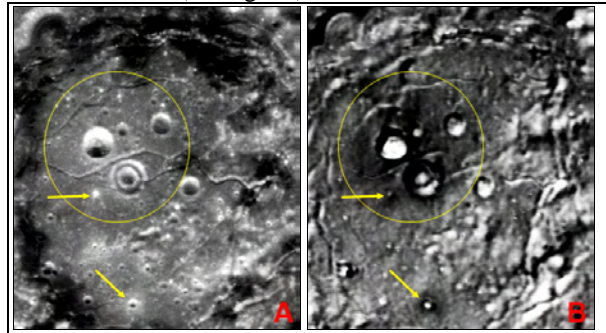


Fig. 2. Reflectance image of the crater Lavoisier (A). Map of phase function steepness  $\eta$  (B). Anomalous outlined areas are discussed in the text.

These old dark lava flows, albeit compositionally different from the crater floor material, have however the same regolithic microstructure as a result of space-weathering processes, and thus do not show up in the  $\eta$  map (Fig. 2b). Two more examples of extended negatively anomalous halos around young small craters are shown with arrows in Fig. 2. The most puzzling feature is the large negative anomaly outlined by the circle around the large craters (4.6 and 5.6 km in size). It might be caused by pyroclastic deposits [8] associated with tectonic fractures across the floor.

**Conclusions:** AMIE preliminary studies reveal new photometric anomalies detected at a typical 100 m/pix resolution. These examples demonstrate the interest of orbital lunar photometry for characterizing the regolith microstructure; it illustrates both the usefulness of spot-pointing imaging observations and the scientific value of the AMIE data set in documenting geological processes associated with floor-fractured craters, pyroclastic deposits and regolith reworking.

**Acknowledgment.** This work is partially supported by CRDF Grant #UKP2-2614-KH-04 and by CNES.

**References:**[1] Kreslavsky M. A. et al. (2000) *JGR*, 105, 20281. [2] Akimov L. A. (1979) *Sov. Astron.*, 23, 231. [3] Pinet P. et al. (2005) *Planet. Space Sci.* 53, 1309. [4] Koschny D. et al (2003) S1-AMIE-RSSD-RP-001. [5] Cerroni P. et al. (2006) *LPSC XXXVII* 1831 [6] Kreslavsky M. A., Shkuratov Y. G (2003) *JGR* 108, 5015. [7] Chevrel S. et al. (1999) *JGR* 104, 16515. [8] Gaddis L. et al. (2000) *JGR* 105, E2, 4245.